Structure of human PRL-3, the phosphatase associated with cancer metastasis ☆

Kyoung-Ah Kim[a], Jin-Sue Song[a], JunGoo Jee[b], Mee Rie Sheen[a], Chulhyun Lee[a], Tae Gyu Lee[c], Seonggu Ro[c], Joong Myung Cho[c], Weontae Lee[d], Toshio Yamazaki[b], Young Ho Jeon[c,*], Chaejoon Cheong[a,*]

[a]*Magnetic Resonance Team, Korea Basic Science Institute, Daejeon 305-333, Republic of Korea*
[b]*Genomic Sciences Center, RIKEN Yokohama Institute, Yokohama 230-0045, Japan*
[c]*The Division of Drug Discovery, CrystalGenomics, Incorporation, Daejeon 305-390, Republic of Korea*
[d]*Department of Biochemistry and HTSD-NMR Laboratory, Yonsei University, Seoul 120-740, Republic of Korea*

Received 20 January 2004; revised 1 March 2004; accepted 15 March 2004

First published online 9 April 2004

Edited by Thomas L. James

Abstract PRL-3, a novel class protein of prenylated tyrosine phosphatase, is important in cancer metastasis. Due to its high levels of expression in metastatic tumors, PRL-3 may constitute a useful marker for metastasis and might be a new therapeutic target. Here, we present the solution structure of the phosphatase domain of a human PRL-3 (residues 1–162) in phosphate-free state. The nuclear magnetic resonance (NMR) structure of PRL-3 is similar to that of other known phosphatases with minor differences in the secondary structure. But the conformation and flexibility of the loops comprising the active site differ significantly. When phosphate ions or sodium orthovanadate, which is a known inhibitor, are added to the apo PRL-3, the NMR signals from the residues in the active site appeared and could be assigned, indicating that the conformation of the residues has been stabilized.

© 2004 Federation of European Biochemical Societies. Published by Elsevier B.V. All rights reserved.

Keywords: PRL-3; Structure; Metastasis; Phosphatase; NMR

1. Introduction

PRL-1, -2, and -3 belong to a novel class of protein tyrosine phosphatases (PTPs) with a C-terminal prenylation motif [1]. These are closely related intracellular enzymes that possess the PTP active site signature sequence HCXXGXXR [2,3]. All three proteins have molecular weights of about 20 kDa and share at least 75% amino acid sequence similarity (Fig. 1).

PRL-1 is localized primarily in the brain and muscle [3]. PRL-2 is preferentially expressed in skeletal muscle, while PRL-3 is found specifically in cardiac and skeletal muscles [3]. PRLs are more homologous to dual-specificity phosphatases (DSPs) than to other tyrosine-specific PTPs, although PRL-1 can dephosphorylate phosphotyrosyl substrate in vitro [2]. Their highest homology is with Cdc14 (20.3%) and with PTEN (16.9%).

To date, the cellular roles of none of the PRLs have been determined. Recent serial analysis of gene expression experiments has shown that PRL-3 is highly overexpressed in liver metastases of colorectal cancer, but not in non-metastatic tumors or in normal colorectal epithelium [4]. Furthermore, causative roles for PRL-3 and -1 in promoting cell motility, invasion activity, and metastasis have been reported [5]. While a catalytically inactive PRL-3 mutant has significantly reduced migration-promoting activity, PRL-3- and -1-expressing cells induce metastatic tumor formation in nude mice. These data strongly suggest that the PRL-3 is important in cancer metastasis and might provide a new therapeutic target for cancer treatment.

Metastasis is the neoplastic process that is responsible for most cancer deaths, as primary tumors can usually be removed surgically. Metastatic cells undergo cytoskeletal changes, loss of adhesion, and enhanced motility, and express proteolytic enzymes that degrade the basement membrane. To understand its mechanism at the atomic level and to discover candidate drugs acting on PRL-3, it is important to determine its three-dimensional structure.

Preliminary nuclear magnetic resonance (NMR) studies of PRL-2 and -3 with backbone assignments have been reported [6,7], and while we were preparing our manuscript, the structure of human PRL-3, solved independently by Kozlov et al. [8], has recently appeared on internet. The structure solved by Kozlov et al. is basically identical to ours except that their structure is a complex structure with a phosphate group whereas ours is an apo structure. When their structure was overlaid on ours, the backbone root mean square deviation of the secondary structure elements was 2.5 Å.

2. Materials and methods

2.1. Expression and purification of the PRL-3 phosphatase domain

PRL-3 (aa 1–162) was cloned into pET21b vector (Novagen Inc., Madison, WI) and overexpressed in *E. coli* BL21(DE3) without tag or fusion sequences. Isotopically enriched PRL-3 was prepared from cells

☆ Supplementary data associated with this article can be found, in the online version, at doi:10.1016/j.febslet.2004.03.062.

* Corresponding authors. Fax: +82-42-865-3419 (C. Cheong); Fax: +82-42-866-9301 (Y.H. Jeon).
E-mail addresses: yhjeon@crystalgenomics.com (Y.H. Jeon), cheong@kbsi.re.kr (C. Cheong).

Abbreviations: NMR, nuclear magnetic resonance; PTP, protein tyrosine phosphatase; DTT, dithiothreitol; DSS, 4,4-dimethyl 4-silapentane sodium sulfonate; DSP, dual-specificity phosphatase

0014-5793/$22.00 © 2004 Federation of European Biochemical Societies. Published by Elsevier B.V. All rights reserved.
doi:10.1016/j.febslet.2004.03.062

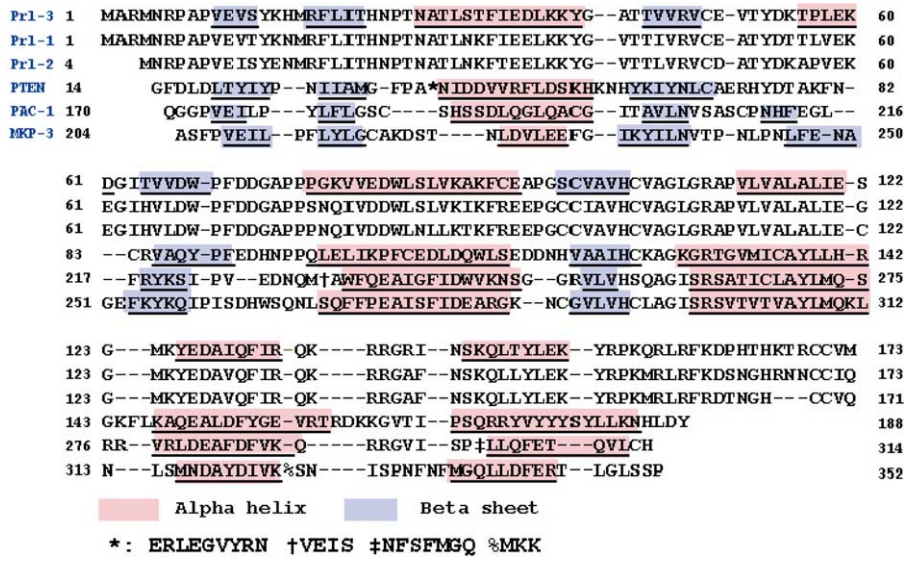

Fig. 1. Structure-based sequence alignment of PRLs, PTEN, PAC-1 and MKP-3. Secondary structure elements are underlined and color-coded.

grown on M9 minimal media containing ^{15}N-ammonium chloride ± ^{13}C-glucose (Cambridge Isotopes Laboratory, Andover, MA). The protein was purified by cation exchange chromatography followed by size-exclusion chromatography. The protein was exchanged into an appropriate buffer and was concentrated to a final concentration of 20 mg/ml.

2.2. NMR spectroscopy

The NMR samples were 1 mM solutions in 50 mM HEPES buffer, 100 mM NaCl, and 10 mM dithiothreitol (DTT) at pH 7.3. The NMR experiments were performed at 303 K on 600 MHz Bruker DRX600 (KBSI and NICEM) and 600 MHz Varian UNITY INOVA (KAIST) spectrometers. The main-chain Cα, Hα, N, NH, and CO and side-chain Cβ resonances were assigned using HNCA, HN(CO)CA, HNCACB, CBCA(CO)NH, HNCO, HN(CA) CO, and HNHA experiments [9]. The side-chain signal assignments were obtained from ^{1}H–^{13}C HSQC, 3D HCCH–COSY, CC(CO)NH, HCC(CO)NH, ^{1}H–^{15}N–HSQC TOCSY, and ^{1}H–^{15}N–HSQC NOESY [10]. The stereospecific assignment of the methyl groups of the Leu and Val residues was achieved with a 20% fractionally ^{13}C-labeled protein dissolved in 99.8% D_2O, as described [11]. Chemical shifts were measured relative to the internal 4,4-dimethyl 4-silapentane sodium sulfonate (DSS) for ^{1}H and calculated for ^{13}C and ^{15}N [12]. Distance information was collected using 3D (^{1}H, ^{13}C) and (^{1}H, ^{15}N) NOESY–HSQC spectra with 100 and 120 ms mixing times. For torsion angle constraints, the backbone vicinal coupling constants ($^{3}J_{HN,H\alpha}$) were estimated from a 3D HNHA spectrum [13] of uniformly ^{15}N-labeled PRL-3.

2.3. Structure calculations

Structures were calculated by CYANA [14] and further refined by AMBER 7 package [15]. All the NOE cross peaks were assigned using CANDID algorithm [16] of CYANA. Totally, 2225 meaningful NOE upper distance restraints were obtained by CANDID. Backbone torsion angle restraints of 143 were derived from HNHA experiment and TALOS program [17] and 27 hydrogen bond restraints from the backbone amides were added as distance restraints in regular secondary structures. With these restraints, final 100 structures were generated using 20 000 time steps of CYANA and further refined by AMBER. AMBER run consisted of 20 ps molecular dynamics, followed by 1500 steps of energy minimization. To approximate solvent interaction, generalized Born model was used [18]. The 20 structures with lowest restraints energy were selected and analyzed using MOLMOL [19], AQUA, and PROCHECK-NMR software [20] (Table 1).

2.4. ^{15}N relaxation measurements

The ^{15}N longitudinal (R_1) and transverse (R_2) relaxation data were collected using eight delays, namely 10–1280 ms for the T_1 experiments and 10–150 ms for the T_2 experiments. The T_1 and T_2 values were determined by fitting the peak heights as a function of the relaxation interval (t) to a two-parameter (I_0 and $R_{1,2}$) exponential decay function, $I(T) = I_0 \exp(-R_{1,2}t)$, using a non-linear least squares analysis.

Table 1
Statistics of PRL-3 final 20 structures[a]

NOE restraints	2225
Intra ($\|i-j\|=0$)	471
Sequential ($\|i-j\|=1$)	609
Medium range ($2 \leqslant \|i-j\| \leqslant 4$)	472
Long range ($\|i-j\| \geqslant 5$)	673
Dihedral angle restraints	143
Hydrogen bond restraints	27×2
Maximum violations	
Distance (Å)	0.22
Angle (°)	3.32
AMBER GB energies (kcal/mol)[b]	
Total	-6588 ± 10
Van der Waals	-1173 ± 13
Electrostatic	$-10{,}750 \pm 403$
Constraints	8 ± 1
Mean deviations from ideal geometry	
Bond lengths (Å)	0.0106 ± 0.0001
Bond angles (°)	2.21 ± 0.02
Coordinate precision (residues 9–158)	
Backbone (Å)	0.76 ± 0.10
Heavy atoms (Å)	1.27 ± 0.13
Ramachandran analysis	
Most favored (%)	83.1
Additionally (%)	13.5
Generously (%)	2.7
Disallowed (%)	0.7

[a] All variation is ±1 S.D. if not specified.
[b] The generalized Born model of AMBER 7.

3. Results and discussion

3.1. Assignment and structure determination

We performed NMR studies on the catalytic domain of PRL-3 (aa 1–162). The C-terminal 11 residues, which include

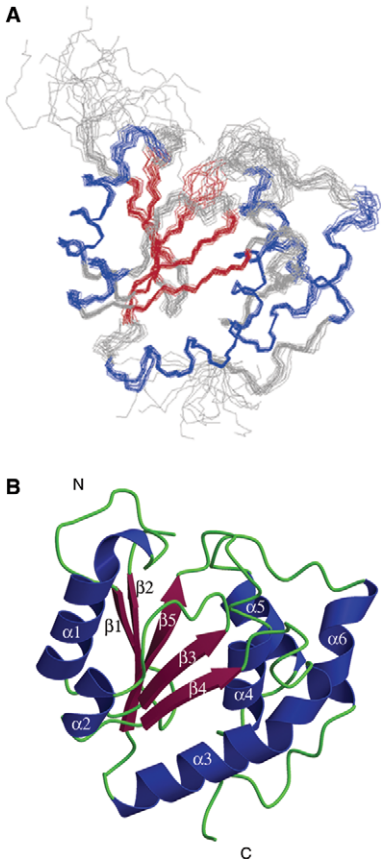

Fig. 2. Structure of PRL-3 derived from NMR experiments. (A) The 20 backbone structures were superimposed. The residues in the helical regions and in the β sheets are shown in *blue* and *red*, respectively. (B) The ribbon diagram of one representative structure.

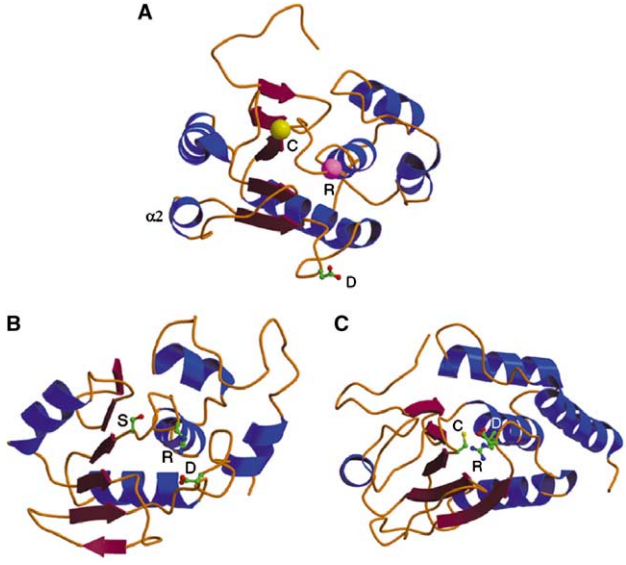

Fig. 3. A comparison of three structures. (A) PRL-3, (B) PAC-1, and (C) PTEN. Residues Cys104 and Arg110 of PRL-3 are marked by filled circles. Asp72 in the general acid loop of PRL-3 and the corresponding residues in PAC-1 and PTEN are shown using a ball-and-stick model.

the prenylation sequence, were truncated to improve solubility. The specific activity of the catalytic domain of PRL-3 was 830 unit/mg/min, which is similar to that of the full-length PRL-3 (730 unit/mg/min) with DiFMUP as substrate [21]. The backbone amide signals of His103 to Ala111 and some of the terminal residues of PRL-3 in the ^{1}H–^{15}N–HSQC spectrum of PRL-3 taken at pH 7.3 could not be detected. Lowering pH down to 6.5 did not make new peaks appear, indicating that missing the amide signals is due to the conformational flexibility. All the backbone amide resonances whose signals could be detected on the HSQC spectra were assigned, and about 97% of the ^{1}H, ^{13}C side-chain of these assigned backbone residues, including aromatic rings, were assigned.

Twenty conformers representing the structure of PRL-3 were calculated from 2422 experimental restraints (the statistics are presented in Table 1). The superimposed backbone traces (N, Ca, C′) of the 20 structures and the ribbon diagram representation of the secondary structure are shown in Figs. 2A and B, respectively. The root mean square deviation of residues 9–158 was 0.76 Å for the backbone and 1.27 Å for the heavy atoms.

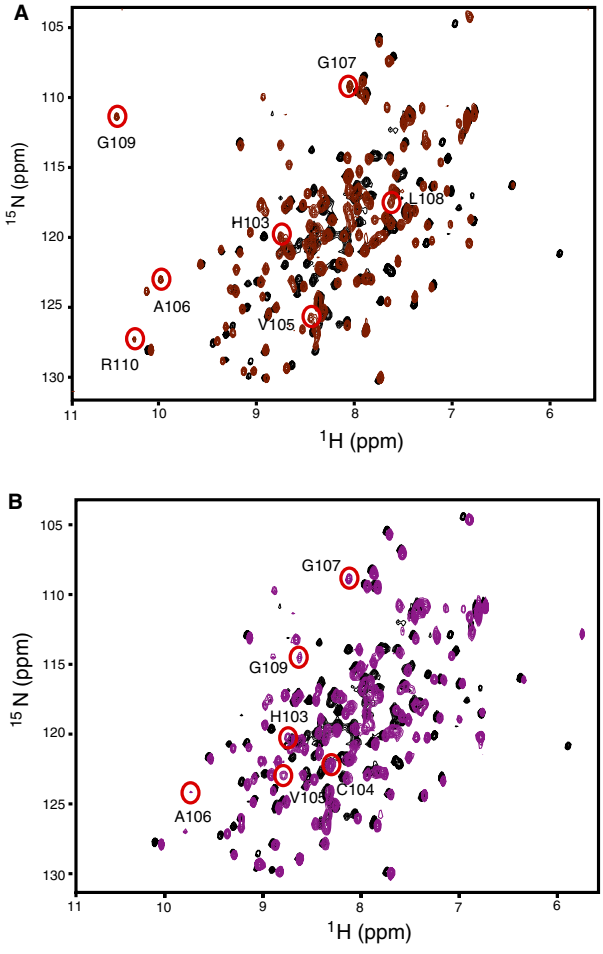

Fig. 4. Overlapping ^{1}H–^{15}N HSQC spectra of PRL-3 obtained in the presence and absence of ligand ions. The peaks representing the free form of the protein are shown in *black*. (A) 0.7 mM PRL-3 with 2 mM sodium orthovanadate (*brown*), (B) 0.7 mM PRL-3 with 20 mM phosphate (*purple*). The *red* circled peaks are the backbone amide protons that appeared in the active site (phosphate loop).

3.2. The structure of PRL-3

PRL-3 has a compact ($\alpha + \beta$) structure comprising a central five-stranded β sheet decorated with six helices, with α1 and α2 on one side and α3 to α6 on the other (Fig. 2B). The molecule exists as a monomer judged by the correlation time of 8.7 ns, which is calculated from the measured T_1 and T_2 values [22]. The location of the enzyme active site is marked by the conserved phosphatase signature sequence HCXXGXXR (residues 103–110), where Cys104 is the enzymatic nucleophile and Arg110 coordinates with the phosphate group on phosphotyrosine (pY). Asp72, which corresponds to Asp226 in PAC-1 and Asp92 in PTEN, is believed to serve as a general acid [23], and is located in the loop connecting β4 and α3. This loop has a characteristic WPFDD sequence. The overall folding topology of PRL-3 is similar to that of the dual specificity phosphatases. The arrangement of the strands within the central β-sheet is in the order 1–2–5–3–4, which is shared by all members of the DSP family including VHR [24], PTEN [25], Cdc14 [26], MKP-3 [27] and PAC-1 [28], except that in the case of the latter two, insertion of an additional β-strand is found between strands 3 and 4. However, the number, orientations, and lengths of the secondary structure elements of PRL-3 are distinct from them.

Fig. 3 compares the structures of PRL-3 (A), PAC-1 (B) and PTEN (C). α2 of PRL-3, which is a relatively short helix between β3 and β4, does not exist in PAC-1 or PTEN. While the overall folding of PRL-3 is similar to the structures of PTEN and PAC-1, the conformation of the loops comprising the active site differs significantly. The side chains of Cys104, Arg110, and Asp72, in PRL-3 are separated from one another, whereas the corresponding residues in PTEN are close together. This structural difference arises mainly from the position of the Asp residue. The general acid loop of PRL-3 is in a very open conformation, thus the Asp residue is not located near the phosphate-binding loop. Whereas, the general acid loop of PTEN is pulled over to the phosphate-binding loop. The case of PAC-1 is midway between PRL-3 and PTEN. Since the three residues, Cys104, Arg110, and Asp72 in PRL-3 should be close together for the enzymatic reaction, a substantial conformational rearrangement of PRL-3 may occur during binding of the substrate molecule.

3.3. Conformational stabilization in the active site

Without any substrate or inhibitor, the phosphate-binding loop between β5 and α4 does not converge well due to a lack of distant constraints. The NMR signals for this region are very weak or undetectable, indicating that a significant conformational exchange is present. To determine whether the conformation of the active site is stabilized on binding of phosphate or known inhibitors, sodium orthovanadate, *p*-nitrophenylphosphate (pNPP), pY and phosphothreonine (pT), 2D NMR titration experiments were conducted in which these ions were added. Fig. 4A shows the changes in the 2D NMR signal of PRL-3 on adding 2.0 mM vanadate ion. New signals

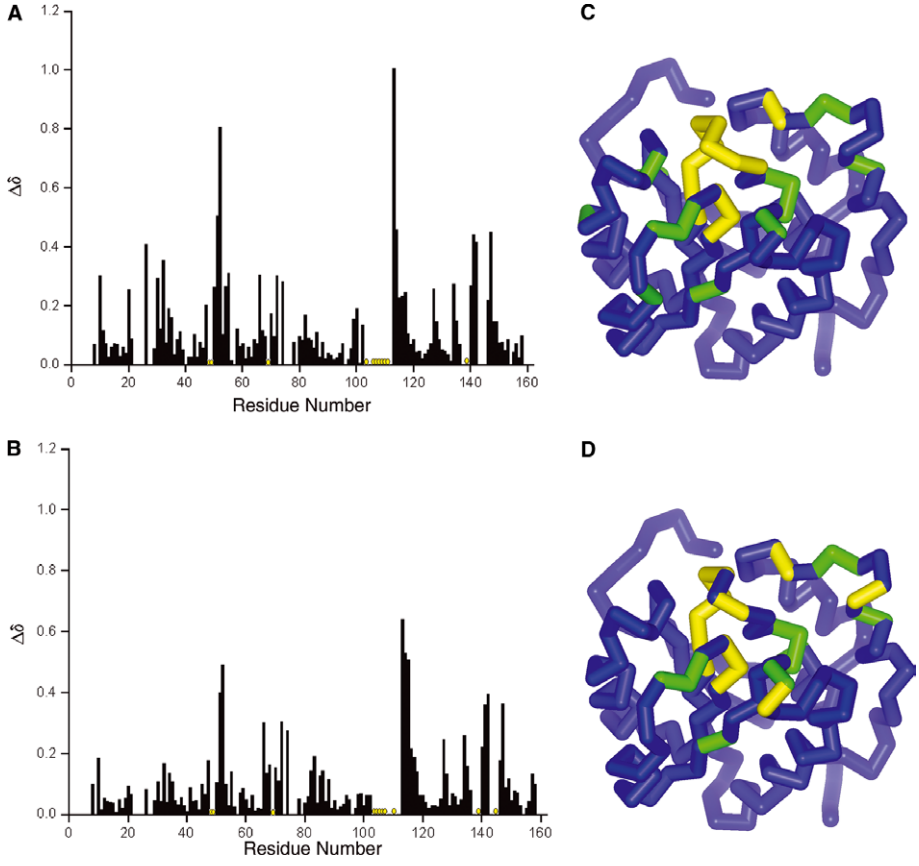

Fig. 5. Weighted average of the ^{15}N and ^{1}H chemical shift perturbations ($\Delta\delta = \sqrt{(\delta H^2 + 0.2 \times (\delta N^2))}$) of PRL-3 on complex formation with ligand ions. Bar diagrams of the perturbations that occurred on addition of 2 mM sodium orthovanadate (A), or 20 mM sodium phosphate (B). Newly appeared peaks are shown as *yellow* circles. The degree of perturbation for vanadate (C) and phosphate (D) is shown in the structure. *Green* residues are perturbed more than 0.3 ppm, *yellow* residues are new in the spectrum, and the remaining residues are *blue*.

from the active site loop region appeared. These were for residues 48, 49, 73, 103, 105–110, and 139. Similarly, 20 mM phosphate ion was added to the PRL-3 solution (Fig. 4B). The new signals that appeared on adding phosphate ions were for residues 48, 49, 73, 103–107, 109, 139, and 145. These signals indicated that the binding of vanadate or phosphate ions stabilizes these parts of PRL-3. Figs. 5A and B summarize the signal changes that occurred on adding vanadate or phosphate ions, respectively. Figs. 5C and D map the residues in PRL-3 that exhibited major resonance changes on addition of vanadate (2 mM) or phosphate (20 mM), respectively. These residues are all located in the loops between β5 and α4, β3 and α2, α5 and α6, and β4 and α3. These loops form the active site cleft of PRL-3. Of note, the vanadate and phosphate ions affect very similar regions of PRL-3. For pNPP, pY and pT, similar results have been obtained (data not shown) indicating that the structural stabilization by the ligand binding is a common phenomenon for these ions.

3.4. Slow- and fast-exchange of vanadate and phosphate ions

The apo-PRL-3 showed significant conformational flexibility around the active site. This type of signal loss indicates that the exchange rate between the different conformers is in the intermediate range compared with the NMR time scale. These lost signals become detectable when phosphate or vanadate ions are added to the protein solution. Farooq and his coworkers reported a similar result for PAC-1 [28]. We assigned the NMR signals that appeared, and found that most of them were from the phosphate-binding loop. Fig. 6A shows a strip plot of the HNCA spectrum of residues 105–110 of PRL-3 with 2 mM vanadate, which demonstrates the backbone NMR signal assignment in this region. The ^{15}N T_1 and T_2 values for the NH of these residues show that after the vanadate ion binds, the residues adopt a stabilized structure, which results in motional parameters similar to those of the rest of the molecule (Fig. 6B). When we analyzed the NMR signals while titrating vanadate ions at concentrations from 0 to 2 mM, several NMR signals clearly showed a slow-exchange pattern on binding of vanadate to PRL-3. Figs. 7A–D show the NMR signal changes in the ^{15}N–^{1}H HSQC spectra due to the serial addition of sodium orthovanadate to the PRL-3 solution. In this case, the original signals from the free form of PRL-3 gradually weakened as new signals from the bound form appeared simultaneously (Figs. 7A–D, see the boxed signals for F33, A74, and A140). This indicates that the exchange rate between the free and bound states is slower than

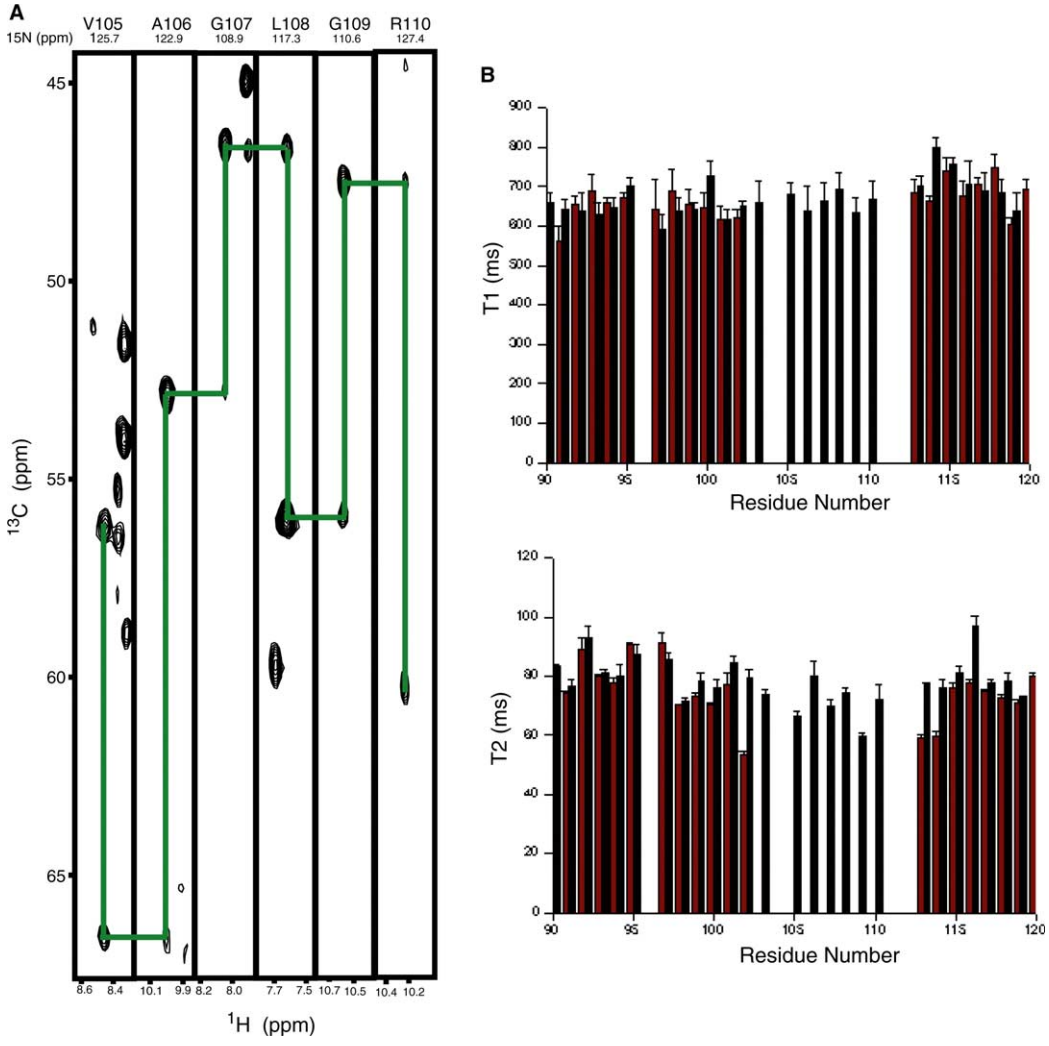

Fig. 6. (A) Strip plot for residues V105 to R110 from the HNCA spectrum of the sodium orthovanadate–PRL-3 complex. (B) ^{15}N T_1 and T_2 values for the residues spanning 90–120 of free PRL-3 (*purple*) and the complex with sodium orthovanadate (*black*).

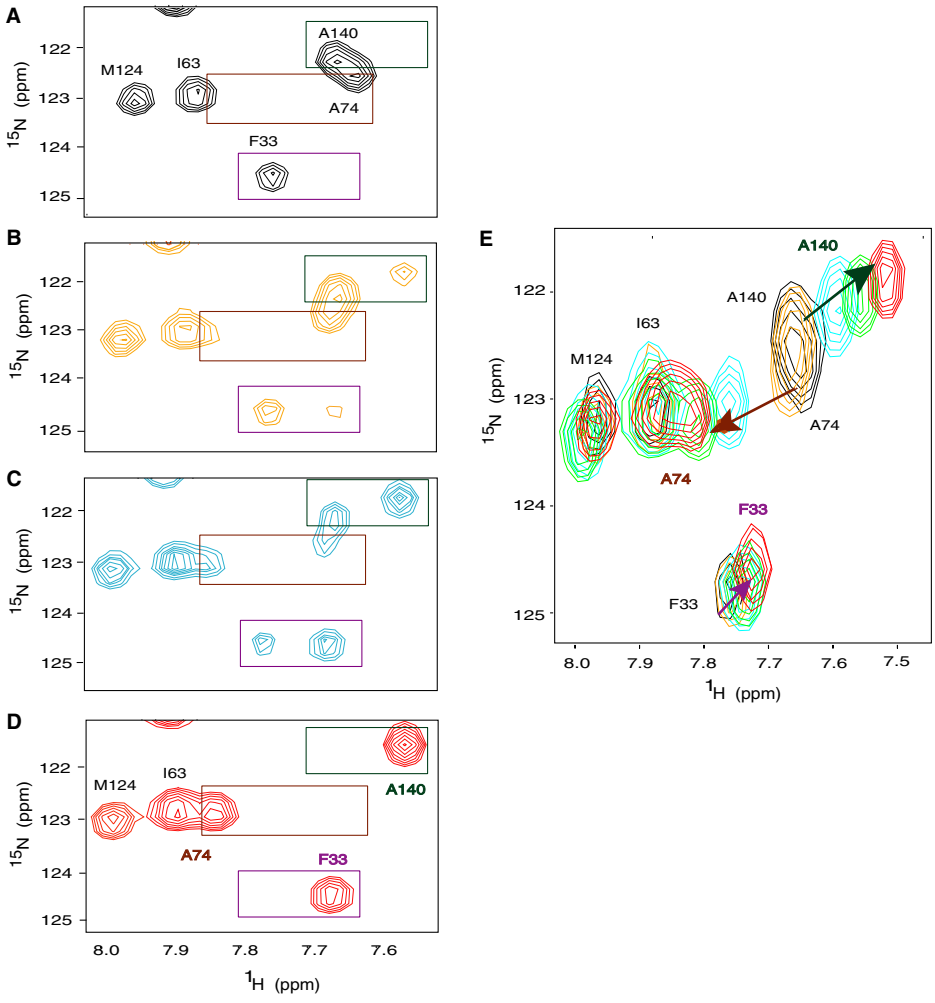

Fig. 7. Peak traces for the ligand titration in ^{1}H–^{15}N HSQC. 2D spectra show the signal changes that occurred on mixing with (A) 0 mM (*black*), (B) 0.5 mM (*orange*), (C) 1.0 mM (*cyan*), or (D) 2.0 mM (*red*) sodium orthovanadate. (E) The shifting path of the peaks (indicated by the arrow) on mixing with 0 mM (*black*), 0.1 mM (*orange*), 1.0 mM (*cyan*), 5.0 mM (*green*), or 20.0 mM (*red*) sodium phosphate.

the time scale of NMR measurement, ca. 30 ms. By contrast, the signals on adding sodium phosphate (Fig. 7E) gradually shifted in one direction until saturation, indicating that the exchange rate of phosphate ion between the free and bound states is faster than the NMR time scale. These observations suggest that vanadate ions bind to PRL-3 in a slow-tight binding pattern, while phosphate ions bind in a fast-weak binding pattern.

3.5. Implication for drug design

The observed structural stabilization and rearrangement that was brought about by the vanadate and phosphate ions suggest that we need to consider conformational flexibility to understand the enzymatic reaction and design an inhibitor. The structural rearrangement suggests that caution should be taken when using a rigid X-ray protein structure in structure-based design studies, as is common in current applications. An alternative strategy is to design an inhibitor that can bind to the inactive conformation and inhibit the structural rearrangement to the active conformation. For example, STI-571, an Abelson tyrosine kinase inhibitor, also known as Gleevec, recognizes the inactive conformation of the kinase and inhibits its activation [29]. Comparing the apo- and ligand-bound structures and considering the possible conformational change that occurs on ligand binding will help us to design potent, selective drug molecules. The PRL-3 structure reported here gives us the three-dimensional features of this new family of PRL phosphatases and will assist in the discovery of anti-cancer drugs that act against this enzyme family.

Acknowledgements: This work was supported by the Consortium Program of the SMBA and by the National Research Laboratory Program of the MOST, the Republic of Korea.

References

[1] Zeng, Q., Si, X., Horstman, H., Xu, Y., Hong, W. and Pallen, C.J. (2000) J. Biol. Chem. 275, 21444–21452.
[2] Diamond, R.H., Cressman, D.E., Laz, T.M., Abrams, C.S. and Taub, R. (1994) Mol. Cell. Biol. 14, 3752–3762.
[3] Zeng, Q., Hong, W. and Tan, Y.H. (1998) Biochem. Biophys. Res. Commun. 244, 421–427.
[4] Saha, S., Bardelli, A., Buckhaults, P., Velculescu, V.E., Rago, C., St Croix, B., Romans, K.E., Choti, M.A., Lengauer, C., Kinzler, K.W. and Vogelstein, B. (2001) Science 294, 1343–1346.

[5] Zeng, Q., Dong, J.-M., Guo, K., Li, J., Tan, H.-X., Koh, V., Pallen, C.J., Manser, E. and Hong, W. (2003) Cancer Res. 63, 2716–2722.
[6] Zhou, H., Gallina, X., Mao, H., Nietlispach, D., Betz, S.F., Fetrow, J.S. and Domaille, P.J. (2003) J. Biomol. NMR 27, 397–398.
[7] Kozlov, G., Cheng, J., Lievre, C., Banville, D., Gehring, K. and Ekiel, I. (2002) J. Biomol. NMR 24, 169–170.
[8] Kozlov, G., Cheng, J., Ziomek, E., Banville, D., Gehring, K. and Ekiel, I. (2004) J. Biol. Chem. 279, 11882–11889.
[9] Bax, A. and Grzesiek, S. (1993) In: NMR of Proteins (Clore, G.M. and Gronenborn, A.M., Eds.), pp. 33–52, MacMillan, London.
[10] Kay, L.E., Xu, G.-Y., Singer, A.U., Muhandiram, D.R. and Forman-Kay, J.D. (1993) J. Magn. Reson. B 101, 333–337.
[11] Hu, W. and Zuiderweg, E.R.P. (1996) J. Magn. Reson. B 113, 70–75.
[12] Wishert, D.S., Bigam, C.G., Yao, J., Abildgaard, F., Dyson, H.J., Oldfield, E., Markley, J.L. and Sykes, B.D. (1995) J. Biomol. NMR 6, 135–140.
[13] Vuister, G.W. and Bax, A. (1993) J. Am. Chem. Soc. 115, 7772–7777.
[14] Güntert, P., Mumenthaler, C. and Wüthrich, K. (1997) J. Mol. Biol. 273, 283–298.
[15] Pearlman, D.A., Case, D.A., Caldwell, J.W., Ross, W.S., Cheatham, T.E., DeBolt, S., Ferguson, D., Seibel, G. and Kollman, P. (1995) Comp. Phys. Commun. 91, 1–41.
[16] Herrmann, T., Güntert, P. and Wüthrich, K. (2002) J. Mol. Biol. 319, 209–227.
[17] Cornilescu, G., Delaglio, F. and Bax, A. (1999) J. Biomol. NMR 13, 289–302.
[18] Xia, B., Tsui, V., Case, D.A., Dyson, H.J. and Wright, P.E. (2002) J. Biomol. NMR 22, 317–331.
[19] Koradi, R., Billeter, M. and Wüthrich, K. (1996) J. Mol. Graph. 14, 29–32.
[20] Laskowski, R.A., Rullmannn, J.A., MacArthur, M.W., Kaptein, R. and Thornton, J.M. (1996) J. Biomol. NMR 8, 477–486.
[21] William, F.M., Thomas, E., Chen, Z., Rama, B., Louis, S., Jeff, D., Brian, J., Laura, B., Todd, P., Mary, D., Susan, A., Raju, J., Vivek, K. and Chris, J.V. (2001) Biochem. Biophys. Res. Commun. 283, 1061–1068.
[22] de la Torre, J.G., Huertas, M.L. and Carrasco, B. (2000) J. Magn. Reson. 147, 136–138.
[23] Rigas, J.D., Hoff, R.H., Rice, A.E., Hengge, A.C. and Denu, J.M. (2001) J. Biol. Chem. 40, 4398–4406.
[24] Yuvaniyama, J., Denu, J.M., Dixon, J.E. and Saper, M.A. (1996) Science 272, 1328–1331.
[25] Lee, J.-O., Yang, H., Georgescu, M.-M., Cristofano, A.D., Maehama, T., Shi, Y., Dixon, J.E., Pandolfi, P. and Pavletich, N.P. (1999) Cell 99, 323–334.
[26] Gray, G.H., Good, V.M., Tonks, N.K. and Barford, D. (2003) EMBO J. 22, 3524–3535.
[27] Farooq, A., Chaturvedi, G., Mujtaba, S., Plotnikova, O., Zeng, L., Dhalluin, C., Ashton, R. and Zhou, M.-M. (2001) Mol. Cell 7, 387–399.
[28] Farooq, A., Plotnikova, O., Chaturvedi, G., Yan, S., Zeng, L., Zhang, Q. and Zhou, M.-M. (2003) Structure 11, 155–164.
[29] Schindler, T., Bornmann, W., Pellicena, P., Miller, W.T., Clarkson, B. and Kuriyan, J. (2000) Science 289, 1938–1942.